ACS APPLIED NANO MATERIALS

www.acsanm.org Letter

Nanoimprinting of Refractive Index: Patterning Subwavelength Effective Media for Flat Optics

Tahmid H. Talukdar, Julius C. Perez, and Judson D. Ryckman*

Cite This: *ACS Appl. Nano Mater.* 2020, 3, 7377–7383 Read Online

ACCESS | Metrics & More | Article Recommendations

ABSTRACT: Subwavelength effective media offer a powerful tool for tailoring optical properties on the surface of a chip but remain challenging to realize at optical frequencies owing to their demand for nanoscale features. To meet this challenge, a simple two-step method for patterning refractive index on the surface of a chip is introduced. The process is referred to as "nanoimprinting of refractive index" (NIRI) and relies on the direct nanoimprinting and plastic deformation of high-porosity mesoporous silicon thin films. This is shown to enable very wide and patternable tuning of refractive index over a range $\Delta n \approx 1$ RIU. Investigation of the effective medium response to film compression reveals close agreement to effective medium theory only after factoring in the contribution from the nanoscaled native oxide. NIRI opens a new route for harnessing the subwavelength degree of freedom and offers the prospect of realizing high-performance and low-cost flat optics.

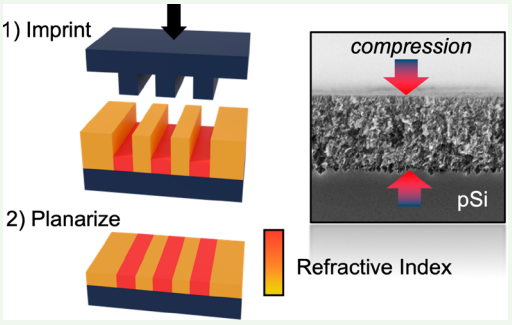

KEYWORDS: *nanoimprinting, porous nanomaterials, gradient refractive index, metasurfaces, flat optics*

Downloaded via CLEMSON UNIV on August 31, 2020 at 19:35:57 (UTC).
See https://pubs.acs.org/sharingguidelines for options on how to legitimately share published articles.

Modern chip-scale photonic devices spanning diffractive,[1] integrated,[2] and meta-optics[3] are typically constructed by structuring a set of homogeneous materials through additive or subtractive processes such as deposition and etching. This affords binary structuring of the refractive index distribution $n(x,y)$ on the surface of a chip and enables a growing gamut of ultrathin and compact photonic device technologies to be fabricated. However, the discrete nature of these platforms poses a significant barrier to realizing arbitrary refractive index patterns and, hence, hinders the development and manufacture of many types of existing and emerging flat-optical devices with novel functionalities.[4−8]

A promising approach to this problem is to fabricate subwavelength structures or gratings that produce an effective medium response.[9−12] However, this task is nontrivial at optical frequencies where subwavelength patterning may demand non-photolithographic techniques such as electron beam lithography[9,13] or focused ion beam milling,[11] which are costly and do not offer high throughput. Composite or graded index media fabricated via polymerization, doping variations, or related methods have also been explored; however, to date their achievable refractive index contrast (e.g., $\Delta n \sim 0.1$) and/or patternability remain very limited.[14−18] Other approaches to locally tailor the refractive index include reconfiguration of an active medium, such as phase change nanomaterials or liquid crystals, which can be programmed to various refractive index states.[19] However, both active and nonvolatile technologies require pixel by pixel addressing, which is challenging to implement over large areas with high resolution and may be subject to elevated environmental sensitivities such as degradation over temperature.[19] Hence, the prospect of arbitrarily patterning refractive indices on the surface of a chip in a scalable process has so far remained elusive.

Mesoporous silicon (pSi) is a composite effective medium comprised of high index silicon which has been electrochemically etched to form pores with tunable diameters ranging from ∼2 to 50 nm. In addition to providing a self-organized subwavelength effective medium without the need for ultrahigh-resolution lithography, it is popular for its low cost and suitability in rapidly prototyping high-quality optical thin films,[20] multilayer waveguides,[21] biosensors,[22] and other optical microstructures such as lenses.[23] Modern pSi devices typically exploit an axial refractive index distribution $n(z)$, which can be tailored over a wide range and with high resolution by modulating the etching current density and thus modulating the local porosity along the etch front as it propagates normal to the chip surface. In plane gradient refractive index variations can be achieved by employing graded current densities[24] or patterned substrate doping;[25] however, these techniques do not foster the development of

Received: May 22, 2020
Accepted: July 2, 2020
Published: July 2, 2020

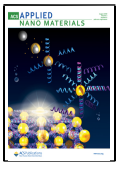

© 2020 American Chemical Society

https://dx.doi.org/10.1021/acsanm.0c01395
ACS Appl. Nano Mater. 2020, 3, 7377–7383

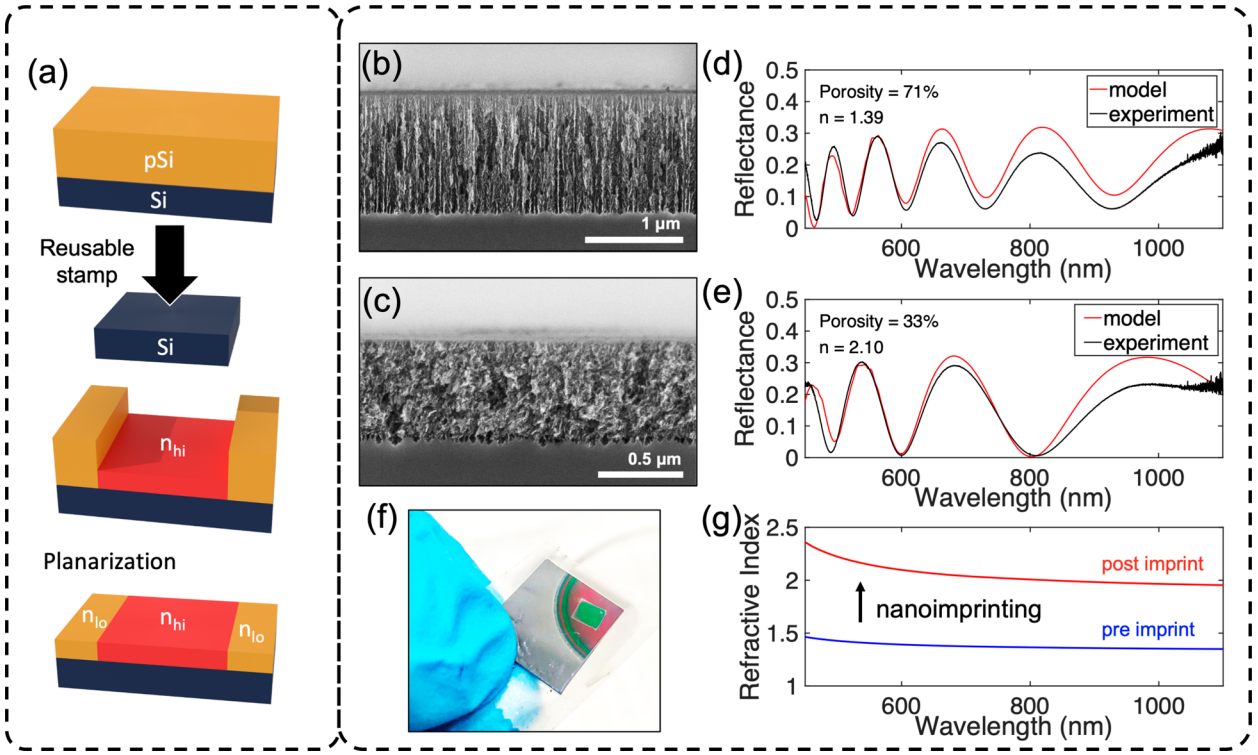

Figure 1. (a) Illustration of NIRI with a flat stamp showing an optional planarization step. (b) SEM image of a preimprinted (~1250 nm) and (c) postimprinted (~550 nm) pSi thin film and (d, e) associated reflectance spectrum fit showing the porosity and refractive index change postimprint. (f) Photograph of a flat imprinted pSi sample showing a clear color change in the imprinted region. (g) Dispersion characteristics of a preimprint and postimprint pSi film.

arbitrary $n(x,y)$ patterns, e.g., with high index contrast and resolution, and would also inherently suffer from the etching induced correlation between local porosity and film thickness.

In this work, we apply direct imprinting of mesoporous silicon (pSi) films[26] as a means for patterning effective refractive indices directly on the surface of a chip in a process we call "nanoimprinting of refractive index" (NIRI). When pressure on the order of ~100 N/mm^2 is applied to high-porosity pSi thin films, localized plastic deformation and compression of the nanostructured silicon skeleton occur. This coincides with a reduction in the local porosity and hence shows an increase in the effective refractive index. In this work, we present an experimental demonstration and characterization of the NIRI process and investigate the effective medium response as a function of the applied film compression. Using the NIRI process, we also demonstrate microscale patterning of refractive index which serves as a proof-of-concept for fabricating flat optics.

The NIRI process is illustrated in Figure 1a. First, pSi thin films are prepared by electrochemical etching of ⟨100⟩ (0.01−0.02 Ω·cm) silicon wafers in 15% ethanoic hydrofluoric acid to create pSi thin films. Current densities of 49.2 and 55.1 mA/cm^2 are applied for 34 and 30 s, respectively, on a circular region of 2.54 cm^2 to create a thin film with a thickness of ~1 μm. The initial film porosities are determined by gravimetric methods to be ~62 ± 5 and ~68 ± 5% for the 49.2 and 55.1 mA/cm^2 etched films, respectively.[27] The imprint process starts by applying a reusable Si stamp with varying pressures ranging from ~75 to 400 N/mm^2, for a duration of ~20−30 s, using a hydraulic press. Panels b and c of Figure 1 show cross-sectional SEM images of an example thin film before and after NIRI. Film compression is measured for all samples by cross-sectional SEM and is herein defined as the fraction $(L_{before} - L_{after})/L_{before}$, where L is the film thickness. After imprinting, the film's refractive index is analyzed by parameter fitting the normal incidence reflection spectra captured from an optical microscope. Our model fit uses the transfer matrix method applied to a single layer film on a silicon substrate and employs a dispersive effective medium model (detailed below) where n and k for silicon and silicon dioxide are given by Palik[28] and Malitson,[29] respectively. The available input parameters to the model fit are the volume fractions for each constituent material (i.e., air, Si, and SiO_2), while the film thickness is set according to the SEM measured value. Here we note that pSi is in general optically anisotropic; however, unlike ⟨110⟩ derived pSi, which exhibits strong birefringence at normal incidence,[30] ⟨100⟩ pSi exhibits zero birefringence at normal incidence owing to the surface normal orientation and rotational disordering of the pores. Hence our work focuses on the refractive index that applies for light propagating at an internal angle near normal to the surface of ⟨100⟩ pSi, a regime which is applicable to a wide variety of prospective flat-optical components.

Panels d and e of Figure 1 report the measured reflectance spectra and a model fit before and after imprinting the same 55.1 mA/cm^2 sample shown in Figure 1b,c. In this example the refractive index is measured to be 1.39 at λ_0 = 600 nm before imprinting, corresponding to an optically determined porosity of ~71%. The sample shown in Figure 1 is imprinted to a film compression of ~0.56, resulting in a significant increase in refractive index to 2.1, which corresponds to a reduced porosity of ~33%. The observed strong fringe contrast and good model fit exemplify the effective medium response of mesoporous silicon thin films, which notably shows negligible scattering losses across the visible spectrum. Figure 1f shows a

https://dx.doi.org/10.1021/acsanm.0c01395
ACS Appl. Nano Mater. 2020, 3, 7377−7383

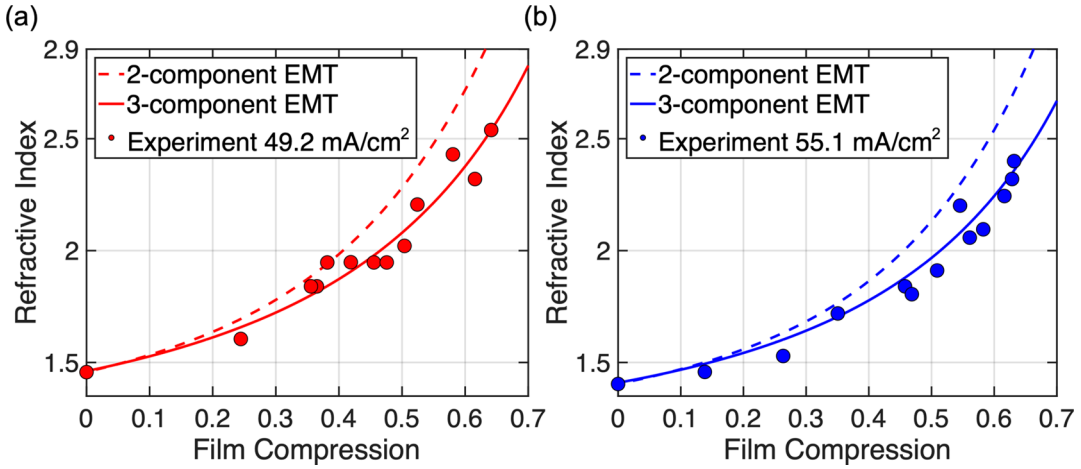

Figure 2. Refractive index vs film compression at λ_0 = 600 nm for gravimetrically determined (a) 62% and (b) 68% starting porosity films.

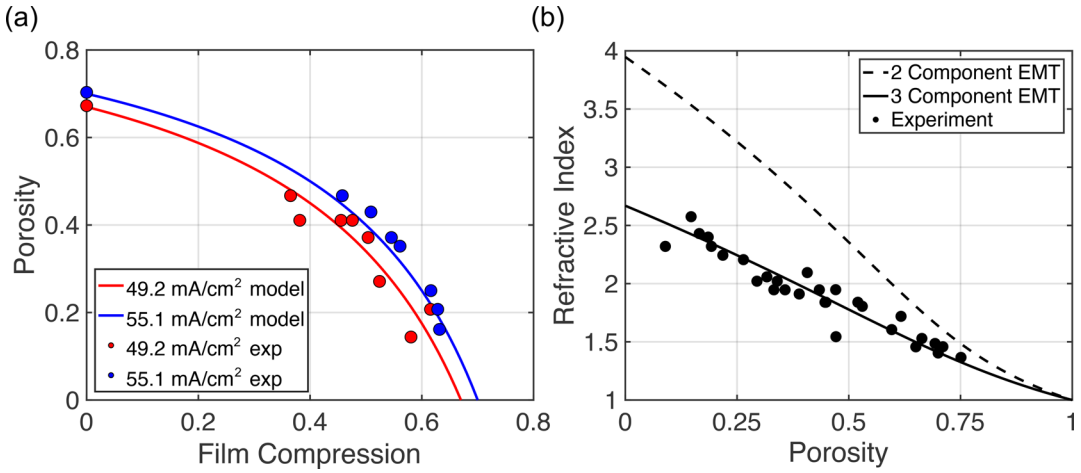

Figure 3. (a) Optically determined porosity vs film compression for pSi films prepared at 49.2 and 55.1 mA/cm^2. (b) Refractive index as a function of porosity for two-component and three-component Bruggeman EMT alongside experimentally measured values wherein porosity is physically determined via gravimetry and SEM. The three-component EMT utilizes a 0.56:0.44 volume ratio of Si:SiO_2 in the porous skeleton.

freshly imprinted pSi sample with a clear color change in the imprinted region. Figure 1g summarizes the refractive index of these two samples over wavelength as determined by fitting to our effective medium model.

By varying the imprint pressure, we generated samples with a wide range of induced film compressions spanning from 0 to 0.65. We note that the theoretical maximum film compression is exactly equal to the starting porosity, as film compression stops when porosity reaches ~0%. If this limit is reached under an applied compressive stress, then film fracture is likely to occur. It is also important to note that the stamp (e.g., Si) should have higher compressive strength than the porous substrate; otherwise, it would deform under applied pressure. Hence the "working range" of film compression should be somewhat less than the starting porosity of the film. Moreover, appropriate imprint leveling and sample cleaning are necessary to ensure uniformity in the applied pressure (e.g., image in Figure 1a) and to avoid that this limit condition is reached in any section of the imprinting area.

Panels a and b of Figure 2 show the measured refractive index at λ_0 = 600 nm as a function of film compression for pSi thin films prepared at 49.2 and 55.1 mA/cm^2. As anticipated, NIRI enables direct control over the refractive index, which increases with increasing film compression. We demonstrate an experimentally achievable refractive index range of $\Delta n \approx 1$ RIU. This offers the prospect of patterning high index contrast flat-optical components through the use of patterned stamps. Crucially, the high-contrast Δn is enabled by working with relatively high porosity pSi substrates which have an initially lower refractive index.

In this study we fit the experimental reflectance spectra with dispersive Bruggeman effective medium theory (EMT) models. Our starting model is a two-component Bruggeman EMT model,[31] which accounts for an effective dielectric function ϵ_{eff} arising from components with dielectric constants ϵ_1 and ϵ_2 according to

$$f_1 \frac{\epsilon_1 - \epsilon_{eff}}{\epsilon_1 + 2\epsilon_{eff}} + (1 - f_1) \frac{\epsilon_2 - \epsilon_{eff}}{\epsilon_2 + 2\epsilon_{eff}} = 0 \quad (1)$$

Here, f_1 and $f_2 = (1 - f_1)$ are the volume fractions associated with ϵ_1 and ϵ_2, respectively. In the literature, pSi is often assumed to be well approximated using a simple two-component system of Si and air. However, this simplistic model is found not to agree with our experimental data as it ignores the non-negligible contribution of the native oxide. To address this issue, we also fit the data to a three-component model (Si−SiO_2−air) that accounts for the native oxide. In this model, we use a nested implementation of eq 1, where at the

https://dx.doi.org/10.1021/acsanm.0c01395
ACS Appl. Nano Mater. 2020, 3, 7377−7383

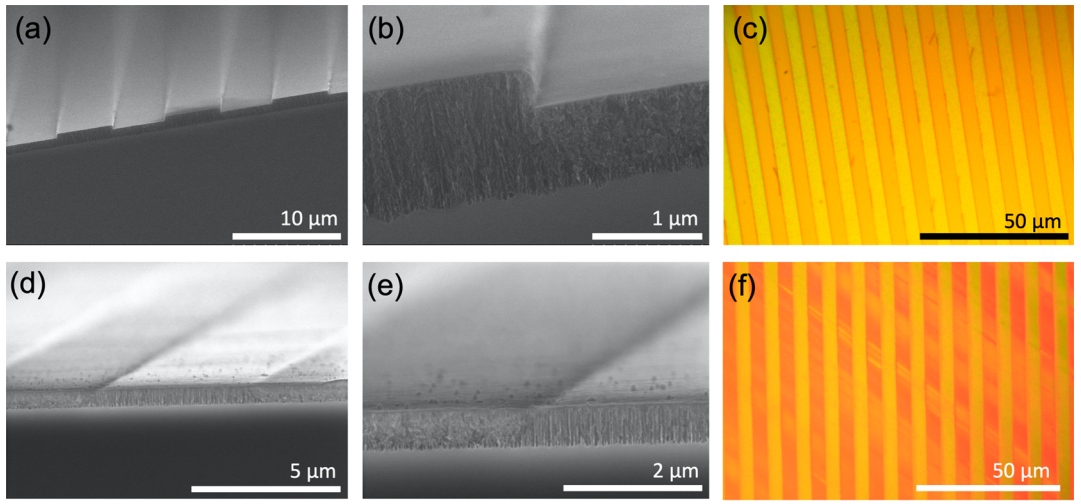

Figure 4. (Top row): SEM images (a, b) and optical microscope image (c) of 49.2 mA/cm^2 1.2 μm sample imprinted with a microscale grating after the NIRI process and (bottom row) after planarization.

top level we consider a two-component system of void (ϵ_1,f_1) and skeleton (ϵ_2,f_2) and at a lower level we consider the skeleton's relative permittivity ϵ_2 to be a two-component system of Si (ϵ_{Si},f_{Si}) and SiO_2 (ϵ_{SiO_2}, f_{SiO_2}), where $f_{SiO_2} = (1 - f_{Si})$ Hence the "porosity" is described by f_1 while the total volume fractions of Si and SiO_2 in a given film are described by $f_{Si}(1 - f_1)$ and $f_{SiO_2}(1 - f_1)$, respectively. The non-negligible nature of the native oxide was further verified by dipping a premeasured pSi sample, which had been aged in ambient conditions for ~3−5 days, in HF to selectively etch away the native SiO_2 inside the pores. After HF exposure the refractive index of the ~55.1 mA/cm^2 film drops by ~0.18, which is attributable to the removal of a ~2 nm SiO_2 layer conformally coating the pores,[32] a thickness which is consistent with a native oxide layer.[33] This highlights the non-negligible impact of the native oxide, which can be accounted for using the three-component EMT. The best fit to our data is obtained for $f_{Si} = 0.56$ and $f_{SiO_2} = 0.44$.

In addition to optically measuring the refractive index and fitting the EMT derived porosity, we also physically measured the porosity via gravimetric methods. Given the one-dimensional nature of the pSi film deformation, which corresponds to a zero Poisson ratio, the evolution of film porosity from its initial state can be predicted as a function of film compression as shown in Figure 3a. In Figure 3a we compare this predicted evolution of porosity vs film compression to the optically determined porosity for each sample according to the three-component EMT. The results indicate excellent agreement between the two. Figure 3b shows the effective refractive index for the two-component (Si−sir) and three-component (Si−SiO_2−air) EMT models. In this graph, the experimental data points report the optically fitted refractive index vs the porosity as determined solely from gravimetry and SEM measurement of film compression. In all cases, it is observed that the two-component model overestimates the refractive index, especially at low porosity (high film compression), and fails to accurately describe the effective medium response of imprinted pSi films. The three-component EMT model closely agrees with the experimental data and best predicts the effective medium response to the NIRI process.

Next, we demonstrate microscale patterning of refractive index in a fully planarized surface using our NIRI technique. Here, a microscale grating is imprinted on a 49.2 mA/cm^2 sample to a film compression of ~0.35, and then the sample is polished in a vibratory polisher (Buehler VibroMet 2) using a 0.05 μm colloidal silica alkaline slurry (pH = 9.8) to achieve a planar surface. SEM and optical microscope images of the film before and after planarization, shown in Figure 4, reveal the high fidelity of the patterning process and confirm the surface relief pattern has been removed while preserving the integrity of the remaining film. As viewed in Figure 4f, the strong index contrast between the imprinted and non-imprinted regions imparts visible structural coloring. Some degree of scratching observed on the surface indicates that the polishing process could be improved by optimizing process conditions. The resulting structure is effectively a flat-optic microscale refractive index pattern which has been achieved without direct writing or subwavelength resolution lithography. We note that earlier work suggests that our imprinting technique can achieve a patterning resolution below 100 nm[26]. In practice we expect this resolution limit to depend on factors such as the aspect ratio of the stamp and the porous film thickness, and hence future experiments to explore the capabilities and limits of NIRI in the sub-micrometer regime are warranted.

This successful proof-of-concept patterning demonstration suggests that application of binary or grayscale stamps[34] with the appropriate surface relief profile could enable NIRI to pattern arbitrarily designed refractive index distributions $n(x,y)$ on the surface of a chip. Our demonstrated dynamic range of refractive indices from ~1.45 to ~2.54 RIU, indicates that flat-optical components with complete 2π phase control can be achieved in films polished to a final thickness of ~300 nm assuming reflection mode operation in the visible. Attractively, the NIRI technique offers access to the subwavelength degree of freedom in a fast and scalable imprinting process which does not require high-resolution lithographic definition of sub-wavelength gratings. This offers the prospect of creating optical structures such as metasurfaces, integrated and transformation optic components, diffractive elements, lenses, structural color patterns, and more—all in a simple two-step process of imprinting and planarization. In principle, our imprinting approach can be extended to a wide range of materials,

https://dx.doi.org/10.1021/acsanm.0c01395
ACS Appl. Nano Mater. 2020, 3, 7377−7383

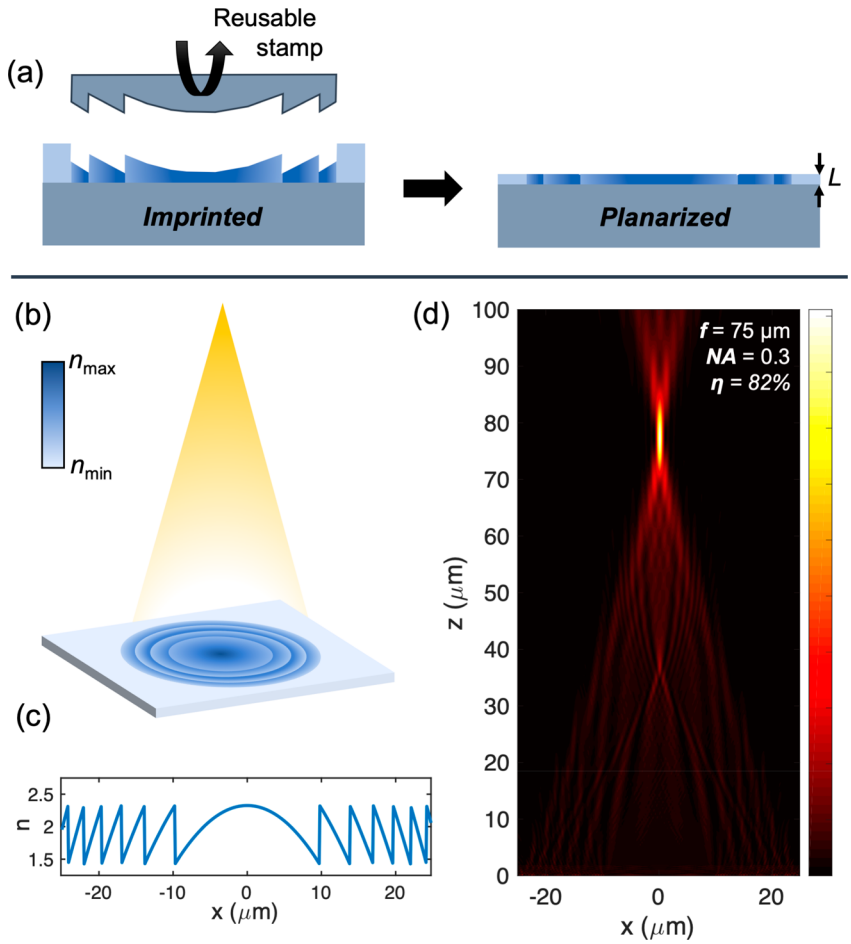

Figure 5. (a) Example illustration of NIRI being applied to realize a truly flat lens, wherein a simple two-step process is used to achieve a desired refractive index profile and film thickness. (b) Illustration of a reflection type diffractive meta-lens prepared on an ideal mirror, and (c) targeted refractive index distribution. (d) FDTD simulation of focusing at λ_0 = 600 nm achieved by the flat lens for a film thickness L = 210 nm.

assuming they can be suitably porosified at the nano- or mesoscale, such as SiO_2, TiO_2, Ge, or Au. Alternative material systems could further widen the prospective applications from the ultraviolet to the mid-infrared. Moreover, a wide number of variants on the NIRI process could be explored in the future, such as transferring the porous film to alternative substrates, infiltrating or inverting the effective medium using deposition and templating techniques, or imprinting ⟨110⟩ pSi to potentially tailor both the refractive index and normal incident birefringence.

Figure 5 illustrates one prospective application of the NIRI process, wherein a grayscale stamp with the appropriate relief pattern is used to achieve a targeted refractive index distribution while planarization is used to achieve a targeted film thickness L. In this example, we consider a polarization insensitive reflection type diffractive meta-lens prepared on an ideal mirror operating at λ = 600 nm, wherein the local optical path length is set by $2n(r)L$, with r indicating the radial distance from the center of the lens. The structure is designed with a wrapped phase profile

$$\phi(r) \propto \mathrm{mod}\left(-\frac{2\pi}{\lambda}(\sqrt{r^2+f^2}-f), 2\pi\right)$$

For a subwavelength film thickness, L = 210 nm, finite difference time domain (FDTD) simulation of a device with the refractive index pattern shown in Figure 5c indicates that it achieves diffraction limited focusing with focal length f = 75 μm and numerical aperture NA = 0.3. The focusing efficiency as measured by the power confined to a radius 3 times the spot's full width at half-maximum is recorded to be η = 82%, which is comparable to state-of-the-art meta-lenses typically fabricated by electron beam lithography and reactive ion etching. We anticipate that this efficiency can be improved through further design optimization. Moreover, this example suggests that a wide variety of flat-optic devices, such as metasurfaces with tailored wavefront control, could be realized using NIRI.

In summary, we have investigated the ability to tailor refractive index through mechanical imprinting of a sub-wavelength effective medium. Our demonstration focuses on a mesoporous silicon platform, which attractively offers high refractive index contrast owing to the high index silicon skeleton and widely tunable porosity. The effective medium response is well described using a three-component (Si−SiO_2−air) Bruggeman effective medium approximation, which importantly factors in the contribution of the native SiO_2. Our NIRI technique offers the potential to realize both existing and novel types of flat-optical components on the surface of a chip in a straightforward, highly tunable, and low-cost process.

https://dx.doi.org/10.1021/acsanm.0c01395
ACS Appl. Nano Mater. 2020, 3, 7377−7383

AUTHOR INFORMATION

Corresponding Author

Judson D. Ryckman − *Holcombe Department of Electrical and Computer Engineering, Clemson University, Clemson, South Carolina 29634, United States;* orcid.org/0000-0001-8125-099X; Email: jryckma@clemson.edu

Authors

Tahmid H. Talukdar − *Holcombe Department of Electrical and Computer Engineering, Clemson University, Clemson, South Carolina 29634, United States;* orcid.org/0000-0002-3664-716X

Julius C. Perez − *Clemson Summer Undergraduate Research Experience Program: Solid State Devices for Electronics, Photonics, and Magnetics Technology, Clemson University, Clemson, South Carolina 29634, United States*

Complete contact information is available at: https://pubs.acs.org/10.1021/acsanm.0c01395

Funding

We acknowledge support from the National Science Foundation (NSF) Awards 1825787 and EEC-1560070.

Notes

The authors declare no competing financial interest.

ACKNOWLEDGMENTS

J.P. and J.R. acknowledge Dr. Rod Harrell for leading the Clemson Summer Undergraduate Research Experience (SURE) program in Solid-State Devices for Electronics, Photonics, and Magnetics Technology which is supported by NSF Award EEC-1560070.

ABBREVIATIONS

EMT, effective medium theory
NIRI, nanoimprinting of refractive index
pSi, porous silicon
RIU, refractive index units
SEM, scanning electron microscopy

REFERENCES

(1) Mohammad, N.; Meem, M.; Shen, B.; Wang, P.; Menon, R. Broadband Imaging with One Planar Diffractive Lens. *Sci. Rep.* **2018**, *8* (1), 2799.

(2) Jahani, S.; Kim, S.; Atkinson, J.; Wirth, J. C.; Kalhor, F.; Noman, A. Al; Newman, W. D.; Shekhar, P.; Han, K.; Van, V.; Decorby, R. G.; Chrostowski, L.; Qi, M.; Jacob, Z. Controlling Evanescent Waves Using Silicon Photonic All-Dielectric Metamaterials for Dense Integration. *Nat. Commun.* **2018**, *9*, 1−9.

(3) Sun, S.; He, Q.; Xiao, S.; Xu, Q.; Li, X.; Zhou, L. Gradient-Index Meta-Surfaces as a Bridge Linking Propagating Waves and Surface Waves. *Nat. Mater.* **2012**, *11* (5), 426−431.

(4) Eskandari, H.; Tyc, T. Controlling Refractive Index of Transformation-Optics Devices via Optical Path Rescaling. *Sci. Rep.* **2019**, *9* (1), 18412.

(5) Tsakmakidis, K. L.; Reshef, O.; Almpanis, E.; Zouros, G. P.; Mohammadi, E.; Saadat, D.; Sohrabi, F.; Fahimi-Kashani, N.; Etezadi, D.; Boyd, R. W.; Altug, H. Ultrabroadband 3D Invisibility with Fast-Light Cloaks. *Nat. Commun.* **2019**, *10* (1), 4859.

(6) Spadoti, D. H.; Gabrielli, L. H.; Poitras, C. B.; Lipson, M. Focusing Light in a Curved-Space. *Opt. Express* **2010**, *18* (3), 3181−3186.

(7) Mohammadi Estakhri, N.; Alù, A. Wave-Front Transformation with Gradient Metasurfaces. *Phys. Rev. X* **2016**, *6* (4), 41008.

(8) Wilkinson, P. B.; Fromhold, T. M.; Taylor, R. P.; Micolich, A. P. Electromagnetic Wave Chaos in Gradient Refractive Index Optical Cavities. *Phys. Rev. Lett.* **2001**, *86* (24), 5466−5469.

(9) Schmid, J. H.; Cheben, P.; Bock, P. J.; Halir, R.; Lapointe, J.; Janz, S.; Delage, A.; Densmore, A.; Fedeli, J.-M.; Hall, T. J.; Lamontagne, B.; Ma, R.; Molina-Fernandez, I.; Xu, D.-X. Refractive Index Engineering With Subwavelength Gratings in Silicon Microphotonic Waveguides. *IEEE Photonics J.* **2011**, *3* (3), 597−607.

(10) Cheben, P.; Halir, R.; Schmid, J. H.; Atwater, H. A.; Smith, D. R. Subwavelength Integrated Photonics. *Nature* **2018**, *560* (7720), 565−572.

(11) Valentine, J.; Li, J.; Zentgraf, T.; Bartal, G.; Zhang, X. An Optical Cloak Made of Dielectrics. *Nat. Mater.* **2009**, *8* (7), 568−571.

(12) Staude, I.; Schilling, J. Metamaterial-Inspired Silicon Nanophotonics. *Nat. Photonics* **2017**, *11* (5), 274−284.

(13) Gharghi, M.; Gladden, C.; Zentgraf, T.; Liu, Y.; Yin, X.; Valentine, J.; Zhang, X. A Carpet Cloak for Visible Light. *Nano Lett.* **2011**, *11* (7), 2825.

(14) Xia, B.; Yan, L.; Li, Y.; Zhang, S.; He, M.; Li, H.; Yan, H.; Jiang, B. Preparation of Silica Coatings with Continuously Adjustable Refractive Indices and Wettability Properties via Sol−Gel Method. *RSC Adv.* **2018**, *8* (11), 6091−6098.

(15) Kang, M.; Sisken, L.; Cook, J.; Blanco, C.; Richardson, M. C.; Mingareev, I.; Richardson, K. Refractive Index Patterning of Infrared Glass Ceramics through Laser-Induced Vitrification [Invited]. *Opt. Mater. Express* **2018**, *8* (9), 2722−2733.

(16) Spahn, P.; Finlayson, C. E.; Etah, W. M.; Snoswell, D. R. E.; Baumberg, J. J.; Hellmann, G. P. Modification of the Refractive-Index Contrast in Polymer Opal Films. *J. Mater. Chem.* **2011**, *21* (24), 8893−8897.

(17) Schäfer, C. G.; Gallei, M.; Zahn, J. T.; Engelhardt, J.; Hellmann, G. P.; Rehahn, M. Reversible Light-, Thermo-, and Mechano-Responsive Elastomeric Polymer Opal Films. *Chem. Mater.* **2013**, *25* (11), 2309−2318.

(18) Franke, H. Optical Recording of Refractive-Index Patterns in Doped Poly-(Methyl Methacrylate) Films. *Appl. Opt.* **1984**, *23* (16), 2729.

(19) Wuttig, M.; Bhaskaran, H.; Taubner, T. Phase-Change Materials for Non-Volatile Photonic Applications. *Nat. Photonics* **2017**, *11* (8), 465−476.

(20) Smith, R. L.; Collins, S. D. Porous Silicon Formation Mechanisms. *J. Appl. Phys.* **1992**, *71* (8), R1.

(21) Talukdar, T. H.; Allen, G. D.; Kravchenko, I.; Ryckman, J. D. Single-Mode Porous Silicon Waveguide Interferometers with Unity Confinement Factors for Ultra-Sensitive Surface Adlayer Sensing. *Opt. Express* **2019**, *27* (16), 22485−22498.

(22) Jane, A.; Dronov, R.; Hodges, A.; Voelcker, N. H. Porous Silicon Biosensors on the Advance. *Trends Biotechnol.* **2009**, *27* (4), 230.

(23) Krueger, N. A.; Holsteen, A. L.; Kang, S. K.; Ocier, C. R.; Zhou, W.; Mensing, G.; Rogers, J. A.; Brongersma, M. L.; Braun, P. V. Porous Silicon Gradient Refractive Index Micro-Optics. *Nano Lett.* **2016**, *16* (12), 7402−7407.

(24) Lorenzo, E.; Oton, C. J.; Capuj, N. E.; Ghulinyan, M.; Navarro-Urrios, D.; Gaburro, Z.; Pavesi, L. Porous Silicon-Based Rugate Filters. *Appl. Opt.* **2005**, *44* (26), 5415−5421.

(25) Kakiuchida, H.; Sekiya, E. H.; Shimodaira, N.; Saito, K.; Ikushima, A. J. Refractive Index and Density Changes in Silica Glass by Halogen Doping. *J. Non-Cryst. Solids* **2007**, *353* (5), 568−572.

(26) Ryckman, J. D.; Liscidini, M.; Sipe, J. E.; Weiss, S. M. Direct Imprinting of Porous Substrates: A Rapid and Low-Cost Approach for Patterning Porous Nanomaterials. *Nano Lett.* **2011**, *11* (5), 1857.

(27) Lai, C.; Li, X.; Liu, C.; Guo, X.; Xiang, Z.; Xie, B.; Zou, L. Improvement in Gravimetric Measurement for Determining the Porosity and Thickness of Porous Silicon Using an Optimized Solution. *Mater. Sci. Semicond. Process.* **2014**, *26*, 501−505.

(28) Palik, E. D., Ed. *Handbook of Optical Constants of Solids*; Academic Press, 1998; Vol. 3.

(29) Malitson, I. H. Interspecimen Comparison of the Refractive Index of Fused Silica. *J. Opt. Soc. Am.* **1965**, *55* (10), 1205−1209.
(30) Hakshur, K.; Ruschin, S. Observation of a Large Optical Birefringence Effect in a (110) Oriented Porous Silicon Layer. *Appl. Phys. Lett.* **2014**, *104* (5), 051909.
(31) Stroud, D. The Effective Medium Approximations: Some Recent Developments. *Superlattices Microstruct.* **1998**, *23* (3−4), 567−573.
(32) Ouyang, H.; Striemer, C. C.; Fauchet, P. M. Quantitative Analysis of the Sensitivity of Porous Silicon Optical Biosensors. *Appl. Phys. Lett.* **2006**, *88* (16), 163108.
(33) Bohling, C.; Sigmund, W. Self-Limitation of Native Oxides Explained. *Silicon* **2016**, *8* (3), 339−343.
(34) Ryckman, J. D.; Jiao, Y.; Weiss, S. M. S. M. Three-Dimensional Patterning and Morphological Control of Porous Nanomaterials by Gray-Scale Direct Imprinting. *Sci. Rep.* **2013**, *3* (1502), 1−7.

https://dx.doi.org/10.1021/acsanm.0c01395
ACS Appl. Nano Mater. 2020, 3, 7377−7383